ARCHIVE OF MECHANICAL ENGINEERING

DOI: 10.24425/ame.2025.157605 2026, Vol. 73, No. 1, pp. 1–17

Tuan Anh NGUYEN [1]

Optimal sliding mode control design using a genetic algorithm for electric power steering control

Received 30 June 2025, **Revised** 13 November 2025, **Accepted** 24 November 2025, **Published online** 20 January 2026

Keywords: electric power steering, genetic algorithm, sliding mode control, vehicle control

This paper presents the design of an optimal robust algorithm for performance control of an automotive electric power steering system. The proposed controller is formulated based on a Sliding Mode Control (SMC) framework. A Genetic Algorithm (GA) with six stages determines the sliding surface parameters of the control mechanism. The Lyapunov criterion evaluates the stability of the system. The novelty of this study lies in integrating the robustness of SMC with the optimization capability of the GA to automatically tune the sliding surface parameters. Unlike conventional SMC designs that rely on manual parameter adjustment, the proposed framework achieves fast convergence and reduced tracking error without complex gain tuning. Furthermore, it simplifies the controller structure and improves energy efficiency while mitigating the chattering phenomenon that typically affects SMC-based systems. The performance of the proposed controller is validated by numerical simulation. The computational results show that tracking errors are significantly reduced (only about 0.101% for v_1 = 30 km/h and 0.132% for v_2 = 60 km/h) compared to conventional PID control. Furthermore, power consumption is also significantly reduced. In addition, the influence of the chattering phenomenon is largely eliminated. This combination can be applied to the control of automotive mechatronic systems.

1. Introduction

Automobiles are widely used today for many purposes, including transporting goods, passengers, and others. A steering system maintains the safety and stability of the vehicle during operation. To reduce steering effort and improve steering feel, ground vehicles are equipped with Power Assisted Steering (PAS). PAS systems are known in three main types: Hydraulic Power Steering (HPS), Electrohydraulic

✉ Tuan Anh NGUYEN, e-mail: anhngtu@tlu.edu.vn

[1] Automotive Engineering Division, Thuyloi University, Hanoi, Vietnam

Power Steering (EHPS), and Electric Power Steering (EPS) [1]. According to Xia and Jiang, the HPS system has been developed since the 1950s and has achieved remarkable achievements over the past six decades [2]. However, this system has limitations, including its bulky size, loud noise during operation, high energy consumption, and lack of environmental friendliness. Therefore, it is usually only equipped on heavy trucks or older vehicles. In [3], Nguyen presented the advantages of the EPS system over the traditional HPS. He suggested that an EPS system could be applied in family cars and small commercial vehicles. Compared with HPS or EHPS, the energy consumption efficiency of the EPS system was significantly improved [4]. According to [5], the assisted torque generated by an assisted motor needed to be increased to ensure the steering efficiency for heavy cars. Therefore, they were usually equipped with two independent motors to maintain the system's stability.

Several studies on EPS control have been published recently. Govender et al. proposed a cascade control structure in [6] for rack position control. This controller was formulated based on two loops: an inner loop with a state space controller and an outer loop with a lead/integrator controller. Although the Bode criterion verified the stability of the system, the desired error was quite large. Hassan et al. presented the design of a Proportional-Integral-Derivative (PID) controller for performance control of a column EPS system (C-EPS) [7]. The control parameters were calculated using a Binary Coded Genetic Algorithm (BCGA) such that the objective function converged to zero. Overall, the algorithm structure was quite simple, and there was no comparison with existing control methods. Two other optimization algorithms called the Ant Colony Optimization (ACO) and the Particle Swarm Optimization (PSO) were introduced in [8] to find the ideal parameters of the PID controller. The computational results showed that the convergence time of the algorithm was relatively early (about 20 iterations for PSO and 40 iterations for ACO). As a result, the energy efficiency was only slightly improved (0.02 to 0.04 A). A fuzzy PI algorithm for the phase compensation objective was introduced in [9]. The PI controller parameters in [9] were tuned through dynamic parameters. The simulation results showed that the EPS performance was improved compared to other conventional control methods. A Back Propagation Neural Network (BPNN) mechanism for tuning PID parameters was proposed in [10]. This method was highly effective in improving the system quality. However, its performance was highly dependent on the vehicle's speed. Recently, Fu et al. introduced a dual-PID control mechanism for controlling the EPS system of large commercial vehicles [11]. Simulation results in [12] showed that the performance of conventional PID control was worse than that of other robust control methods. Zhao et al. compared PID control, H_2 control, and H_∞ control. In general, the performance of traditional PID controllers could not meet system stability requirements [13].

PID control only applies to systems formed by one input and one output. Irmer and Henrichfreise proposed the Linear Quadratic Regulator (LQR) design for controlling the EPS system [14]. The output signals were observed through Linear

Quadratic Estimation (LQE). However, the description of the algorithmic structure was incomplete. Furthermore, the method for selecting the optimal parameters was absent. Inspired by the natural selection process, Liu et al. proposed using the GA to find the ideal parameters for the system [15]. A Linear Parameter-Varying (LPV) control mechanism based on H_2/H_∞ PI observer was proposed in [16] to enhance the EPS quality. In general, the performance of linear control methods was degraded under severe operating conditions compared to robust nonlinear control methods [17].

Several robust control methods have shown high efficiency in controlling automotive EPS systems. Nguyen introduced a combination of a Backstepping Control (BSC) technique with fuzzy PI to eliminate steady-state errors [18]. This method was applied to simple (formed by a linear dynamic model) and complex (formed by a nonlinear dynamic model) systems [19]. However, the linearization of some equations during the calculation process led to errors in practice. A robust control mechanism based on Active Disturbance Rejection Control (ADRC) was presented in [20]. However, the performance improvement was slight. Another study by Na et al. showed that the output signals were negatively affected by chattering when the system was directed by the ADRC mechanism [21].

A robust control method for the nonlinear object is known as the Sliding Mode Control (SMC). In [22], Kim et al. proposed using a SMC mechanism for the EPS model based on a disturbance observer. An experiment was conducted to verify the performance of the system. Lee et al. designed an adaptive SMC mechanism to control steering wheel torque tracking [23]. Although the tracking error was improved, the chattering phenomenon occurred strongly, leading to the degradation in system performance [22, 23]. An adaptive fuzzy SMC mechanism for reducing the influence of chattering was proposed in [24]. Some solutions for combining SMC with PID or SMC with BSC to eliminate the influence of chattering were introduced in [3, 25]. Several robust fuzzy SMC and predictive SMC applications have shown high effectiveness in controlling various mechatronic systems [26–28]. In general, the structure of the above algorithms was quite complicated.

Despite the progress achieved in EPS control, several challenges remain. Conventional control techniques such as PID, LQR, or fuzzy-PI generally suffer from performance degradation when the system operates under nonlinear or rapidly varying conditions. Although SMC provides strong robustness, it often causes severe chattering and may not fully guarantee convergence in all operating regions. Meanwhile, many advanced hybrid or intelligent approaches proposed in recent studies possess highly intricate mathematical structures, which make them difficult to tune and implement in real-time applications. These limitations motivate the development of a more compact and optimally tuned robust control strategy that ensures both stability and practical feasibility under complex driving scenarios.

This paper introduces an optimal and robust control strategy to address the existing limitations. The proposed approach is built upon the SMC framework, while the GA is employed to automatically determine the sliding surface parameters.

This integration reduces tracking errors, suppresses chattering, and simplifies the parameter-tuning process.

The key contributions of this work can be summarized as follows.

- A GA-based SMC structure is established, enabling automatic optimization of the sliding surface parameters for minimal tracking error and improved robustness.
- The control law is formulated concisely and computationally efficient to facilitate real-time implementation.
- A unified algorithmic framework is presented to connect the GA optimization process with SMC dynamics, allowing the method to be readily extended to other automotive mechatronic systems.
- Extensive simulations demonstrate that the proposed approach achieves higher accuracy, enhanced stability, and lower power consumption than conventional PID schemes.

The content of the paper is organized into four sections. The literature review and research gaps are presented in the first section. The following section shows the mathematical model of the system. The performance of the proposed approach is confirmed by simulation, which is described in the next section. The conclusion section presents the achievements and some remaining drawbacks.

2. Mathematical models

The EPS systems are commonly divided into 3 types, depending on the position of the assisted motor: column (C-EPS), rack (R-EPS), and pinion (P-EPS). This paper only deals with the model of the C-EPS system. The structure of a standard C-EPS system is shown in Fig. 1, including the steering column, steering wheel, a

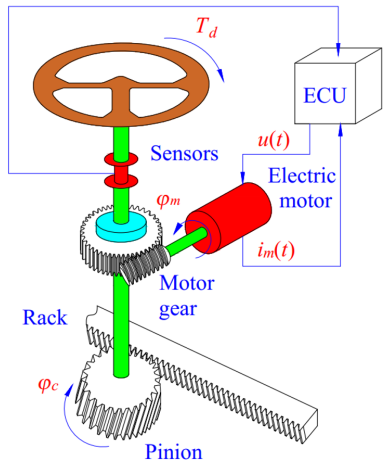

Fig. 1. EPS structure

pair of motor gear, rack and pinion, sensors, assisted motor, and Electronic Control Unit (ECU).

The relationship between the steering motor angle and the steering column angle is shown in following equations:

$$J_c\ddot{\varphi}_c + B_c\dot{\varphi}_c + K_c\varphi_c = \frac{K_c}{N}\varphi_m + T_d\,, \tag{1}$$

$$\frac{K_c}{N}\varphi_c + K_t i_m - \frac{T_r}{N} = J_{\text{eq}}\ddot{\varphi}_m + B_{\text{eq}}\dot{\varphi}_m + \frac{K_c + K_r r_p^2}{N^2}\varphi_m\,, \tag{2}$$

$$K_t\dot{\varphi}_m + L_m\dot{i}_m + R_m i_m = u(t), \tag{3}$$

$$J_{\text{eq}} = J_m + \frac{r_p^2}{N^2}M_r\,, \tag{4}$$

$$B_{\text{eq}} = B_m + \frac{r_p^2}{N^2}B_r\,, \tag{5}$$

where φ_c is steering column angle, φ_m is steering motor angle, i_m is assisted motor current, B_c is steering column damping, B_m is steering motor damping, B_r is rack damping, B_{eq} is equivalent damping, J_c is the inertia moment of the steering column, J_m is the inertia moment of the steering motor, J_{eq} is the equivalent inertia moment, K_t is torque coefficient, r_p is pinion radius, R_m is motor resistance, L_m is motor inductance, N is motor gear ratio, M_r is rack mass, T_d is driver torque, T_r is road reaction torque, and $u(t)$ is control signal.

Driver torque (T_d) is generated by the driver's effort and is considered known. In contrast, road reaction torque (T_r), considered a disturbance, must be calculated using a dynamic model. The variation of T_r can be approximated by equation (6), where d_c is caster trail, d_n is knuckle arm distance, λ is kingpin angle, θ is caster angle, and T_{dis} is the environmental disturbance.

$$T_r \approx r_p d_c \frac{\cos^2(\lambda)\cos^2(\theta)}{d_n}F_{y1} + T_{\text{dis}}\,, \tag{6}$$

$$F_{yi} = -C_{\alpha i}\alpha_i\,, \tag{7}$$

$$\alpha_i = \frac{v_y + (-1)^{i-1}d_i\dot{\psi}}{v_x} - \delta_i\,. \tag{8}$$

Lateral tire force (F_y) is approximated by (7) where C_α denotes stiffness and α is the lateral slip angle. Equation (8) shows how to determine the lateral slip angle, where v_x is longitudinal velocity, v_y is lateral velocity, ψ is yaw angle, δ is steering angle, and d_i are axle distances. The relationship between v_y and v_x is denoted by β and is expressed by equation:

$$\beta = \arctan\frac{v_y}{v_x}\,. \tag{9}$$

The yaw angle is determined by equations (10) to (12), where J_ψ is the yaw inertia moment. These equations are formulated according to a linear dynamic model (Fig. 2):

$$m\left(\dot{v}_x - \dot{\psi} v_y\right) = F_{x1}\cos\delta + F_{x2} - F_{y1}\sin\delta\,, \tag{10}$$

$$m\left(\dot{v}_y - \dot{\psi} v_x\right) = F_{y1}\cos\delta + F_{y2} + F_{x1}\sin\delta\,, \tag{11}$$

$$J_\psi \ddot{\psi} = \left(F_{x1}\sin\delta + F_{y1}\cos\delta\right) - d_2 F_{y2}\,. \tag{12}$$

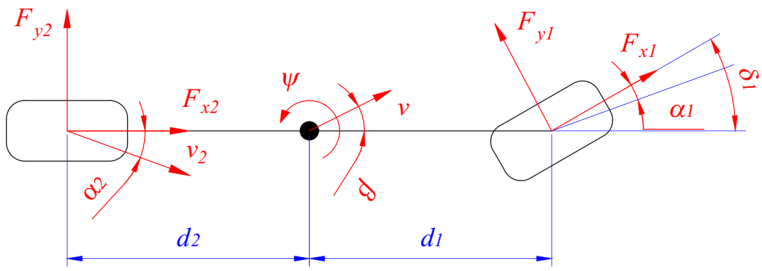

Fig. 2. Vehicle dynamics model

An SMC control mechanism is proposed in this work. Let the state variables be in order:

$$\left[x_i\right]^{\mathrm{T}} = \left[\varphi_c \quad \dot{\varphi}_c \quad \varphi_m \quad \dot{\varphi}_m \quad i_m\right]^{\mathrm{T}}. \tag{13}$$

Taking their derivatives, we get:

$$\dot{x}_1 = x_2\,, \tag{14}$$

$$\dot{x}_2 = -\frac{K_c}{J_c}x_1 - \frac{B_c}{J_c}x_2 - \frac{K_c}{J_c N}x_3 - \frac{T_d}{J_c}\,, \tag{15}$$

$$\dot{x}_3 = x_4\,, \tag{16}$$

$$\dot{x}_4 = \frac{K_c}{J_{\mathrm{eq}}N}x_1 - \frac{K_c + K_r r_p^2}{J_{\mathrm{eq}}N^2}x_3 - \frac{B_{\mathrm{eq}}}{J_{\mathrm{eq}}}x_4 + \frac{K_t}{J_{\mathrm{eq}}}x_5 - \frac{T_r}{J_{\mathrm{eq}}N}\,, \tag{17}$$

$$\dot{x}_5 = -\frac{K_t}{L_m}x_4 - \frac{R_m}{L_m}x_5 - \frac{1}{L_m}u(t). \tag{18}$$

The steering motor angle is the controlled object and is denoted by y, according to equation (19).

$$y = x_3\,. \tag{19}$$

Taking the derivative of equation (19) many times, we get equations (20)–(22). The symbols a_i are explained according to equations (23) to (27).

$$\dot{y} = x_4\,. \tag{20}$$

$$\ddot{y} = \frac{K_c}{J_{\text{eq}}N}x_1 - \frac{K_c + K_r r_p^2}{J_{\text{eq}}N^2}x_3 - \frac{B_{\text{eq}}}{J_{\text{eq}}}x_4 + \frac{K_t}{J_{\text{eq}}}x_5 - \frac{T_r}{J_{\text{eq}}N}, \tag{21}$$

$$\ddot{y} = \sum_{i=1}^{5} a_i x_i + f\left(T_r, \dot{T}_r\right) + \frac{K_t}{J_{\text{eq}}L_m}u(t) = a(x) + bu(t), \tag{22}$$

$$a_1 = -\frac{B_{\text{eq}}K_c}{J_{\text{eq}}^2 N}, \tag{23}$$

$$a_2 = \frac{K_c}{J_{\text{eq}}N}, \tag{24}$$

$$a_3 = \frac{B_{\text{eq}}\left(K_c + K_r r_p^2\right)}{J_{\text{eq}}^2 N^2}, \tag{25}$$

$$a_4 = -\frac{K_c + K_r r_p^2}{J_{\text{eq}}N^2} - \frac{B_{\text{eq}}}{J_{\text{eq}}} - \frac{K_t^2}{J_{\text{eq}}L_m}, \tag{26}$$

$$a_5 = -\frac{B_{\text{eq}}K_t}{J_{\text{eq}}^2} - \frac{K_t R_m}{J_{\text{eq}}L_m}. \tag{27}$$

The error between the reference and real signals is denoted by e, according to equation (28). Taking the third derivative of (28), we get equation (29).

$$e = x_{3\text{ref}} - x_3, \tag{28}$$

$$\ddot{e} = \dddot{x}_{3\text{ref}} - \dddot{x}_3 = \dddot{x}_{3\text{ref}} - \dddot{y}. \tag{29}$$

A linear sliding surface (σ) is chosen according to equation (30); k_1 and k_2 are constants to satisfy the Hurwitz stability condition. Equation (31) is obtained by taking the derivative of the sliding surface.

$$\sigma = \ddot{e} + k_1\dot{e} + k_2 e, \tag{30}$$

$$\dot{\sigma} = \dddot{e} + k_1\ddot{e} + k_2\dot{e}. \tag{31}$$

Equation (32) provides information about the choice of a Lyapunov control function, satisfying the condition of being positive definite. Taking the derivative of $V(x)$, we get (33).

$$V(x) = \frac{1}{2}\sigma^2, \tag{32}$$

$$\dot{V}(x) = \sigma\dot{\sigma}. \tag{33}$$

Substituting equations (22), (29), and (31) into (33), we get:

$$\dot{V}(x) = \sigma\left(\dddot{x}_{3\text{ref}} - a(x) - bu(t) + k_1\ddot{e} + k_2\dot{e}\right). \tag{34}$$

The control signal $u(t)$ is chosen as (35), with K being a positive constant. Combining equations (34) and (35), we get (36). Combining (32) and (36), the system is considered stable.

$$u(t) = \frac{1}{b}\left[-a(x) + \ddot{x}_{3\text{ref}} + k_1\ddot{e} + k_2\dot{e} + K\text{sat}(\sigma)\right], \tag{35}$$

$$\dot{V}(x) = -\sigma K\text{sat}(\sigma). \tag{36}$$

Choosing coefficients k_1 and k_2 is crucial because it affects the system's performance. In this paper, we propose using GA to determine the control parameters. An algorithmic flowchart is presented in Fig. 3, which consists of six stages [29]. The evaluation and initialization process is performed in the first stage. The initial values are determined in this stage and are listed in Table 1. The goal of this work is to find the optimal parameters. This goal is changed to finding the extrema of the function $F(\vartheta)$, described in (37), to simplify the optimization calculation.

$$\vartheta = \begin{bmatrix}\vartheta_1 & \vartheta_2 & \dots & \vartheta_n\end{bmatrix}^{\text{T}}. \tag{37}$$

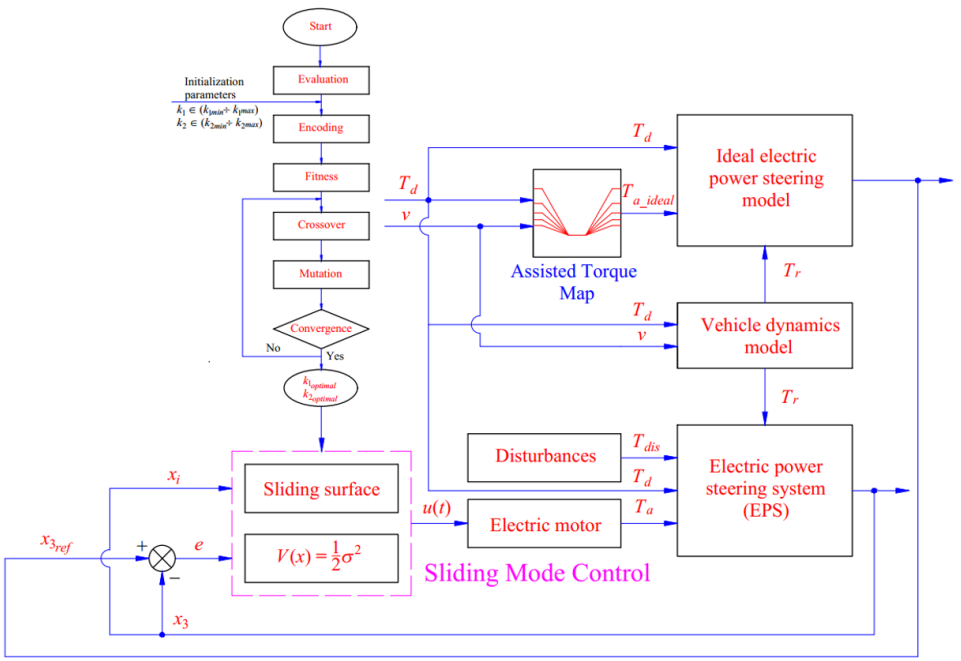

Fig. 3. Algorithmic flowchart

The solution of the extremum problem is then encoded into chromosome strings in the second stage. In this work, we propose a binary encoding method to speed up the computation. A natural selection process is performed to find

Table 1. Initialization parameters

Parameters	Value
Generation number	1000
Population size	20
Stall generation number	700
Mutation probability	0.1
Crossover probability	0.9

individuals with high fitness. These individuals are identified by finding the fitness of the function $F(\vartheta)$, according to calculation.

$$J(\vartheta) = \text{fitness}\big(F(\vartheta)\big). \tag{38}$$

The crossover process is carried out in the next stage. A two-point crossover method is proposed for this purpose. Offspring chromosomes are formed by combining the parental chromosome segments. The mutation process occurs in the fifth stage. According to equation (39), the mutation probability (a_M) is inversely proportional to the length of the chromosome chain (L_c). The value of a_M should be chosen appropriately to avoid population disturbance.

$$a_M \sim L_c^{-1}\,. \tag{39}$$

The obtained results are compared to determine their convergence. The computation stops only when the optimal values are found, i.e., those that minimize the tracking error, according to equation (40).

$$e \xrightarrow{\text{convergence}} \text{Minimum} \rightarrow \begin{cases} k_{1\text{optimal}} \\ k_{2\text{optimal}} \end{cases}. \tag{40}$$

In general, the algorithmic information flow is described as follows:

Step 1: Initialize GA parameters (population size, generation number, crossover, and mutation probabilities).

Step 2: Generate an initial population of sliding surface parameters.

Step 3: For each individual, compute the fitness function.

Step 4: Apply selection, crossover, and mutation to form a new population.

Step 5: Update and evaluate the new population until the termination criteria are satisfied.

Step 6: Use the optimal parameters obtained to construct the SMC law and validate performance through simulation.

This procedure links the optimization and control design processes, allowing reproducibility for similar applications.

3. Simulations

The quality of the proposed controller is confirmed by simulation. The system specifications are mentioned in Table 2.

Table 2. Vehicle specifications

Symbol	Value	Unit	Symbol	Value	Unit
J_c	0.062	kgm^2	J_m	0.0004	kgm^2
B_c	0.063	Nms/rad	B_m	0.0043	Nms/rad
K_c	130	Nm/rad	d_c	0.03	m
N	18.5	–	d_n	0.3	m
K_t	0.05	Nm/A	θ	3	°
r_p	0.005	m	λ	10	°
M_r	28	kg	C_α	35500	N/rad
R_m	0.46	Ω	d_i	1.2/1.6	m
B_r	3300	Ns/m	m	1400	kg
L_m	0.005	H	J_ψ	3060	kgm^2

The change in driver torque is illustrated in Fig. 4a, and the effect of environmental disturbances is shown in Fig. 4b.

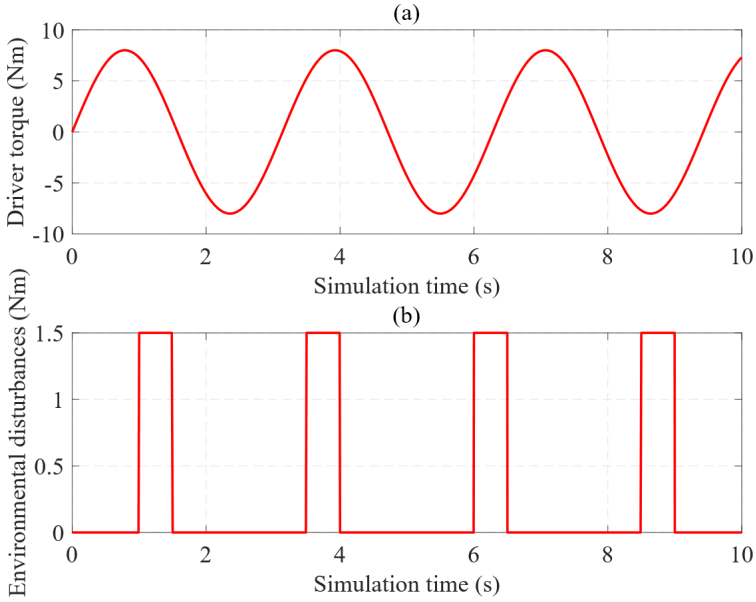

Fig. 4. Known inputs: (a) driver torque, (b) environmental disturbances

Simulation is performed for two cases: v_1 = 30 km/h and v_2 = 60 km/h. The results from the proposed controller (SMC-GA) are compared with those of PID and the reference control. Some symbols mentioned in the following figures are explained: SCA is steering column angle, SCS is steering column speed, SMA is steering motor angle, and SMS is steering motor speed.

3.1. Steering at speed v_1

Fig. 5 shows the output variation over time when the car moves at low speed v_1 = 30 km/h). Looking at Fig. 5a, one can see that the SCA signal tends to change according to the steering law with different errors. If the system has a failure, the RMS error increases to 3.034. Regarding the system controlled by the conventional PID controller, the RMS error is 0.319 rad. In contrast, the tracking error is significantly reduced to 0.004 rad once the SMC-GA method is utilized to control the system.

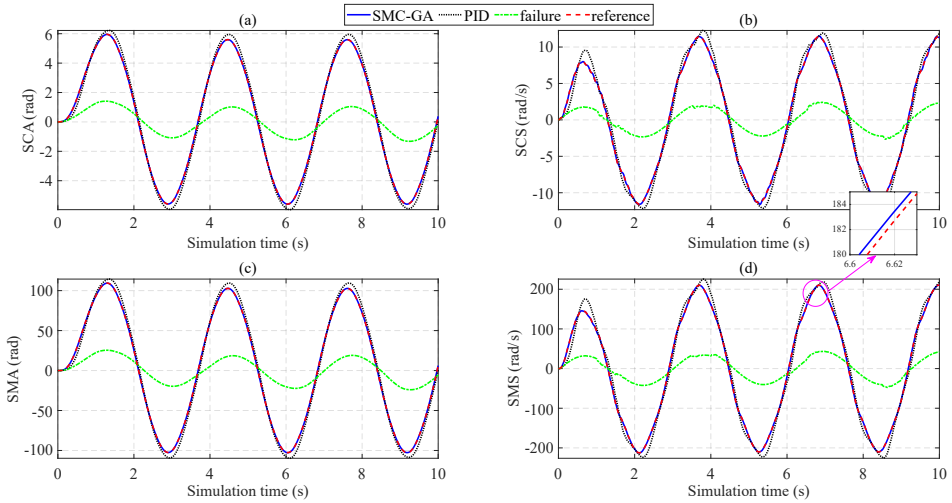

Fig. 5. Change in outputs over time (v_1): (a) SCA value; (b) SCS value; (c) SMA value; (d) SMS value

Under the influence of environmental disturbances, the SCS signals are slightly vibrated, causing the error to increase (Fig. 5b). According to the calculation results, the RMS error of the PID controller is 11.248%, which is much higher than that of the proposed controller (only 0.840%). A sharp decline in performance is seen when the control system fails, causing the RMS error to increase to 80.274%.

The value of SMA is more significant than SCA's, while their changing trends are similar (Fig. 5c). The calculation results show a slight tracking error, only about 0.101% when the SMC-GA technique controls the EPS system. In contrast, this value increases to 8.299% when the traditional PID technique is applied to control the object. The window plot in Fig. 5d shows that the RMS error between SMC-GA

and reference signals is negligible, while the error of the traditional PID controller is up to 11.080%. Overall, the signals obtained by the proposed controller follow the reference signal with high accuracy.

The assisted motor current and assisted torque evaluate the power-assisted performance of the steering system. The variation of the assisted motor current (i_m) is illustrated in Fig. 6a with three signals: SMC-GA, PID, and the reference. The motor current obtained by the proposed controller tracks the reference signal better than that of the PID controller. At some points, the signal overshoots. This is due to the excitation by environmental disturbance pulses (Fig. 4b). The calculation results show that the RMS error of the PID controller can reach 24.241%, while that of the SMC-GA is only 9.426%. The influence of the assisted torque on the driver torque is illustrated in Fig. 6b. The value of the assisted torque rises as the driver torque rises, and vice versa. This value reaches saturation once the driver torque exceeds its maximum limit. The signal obtained by the SMC-GA controller tracks the reference signal with a small error. These findings aid in showcasing the effectiveness of the suggested controller.

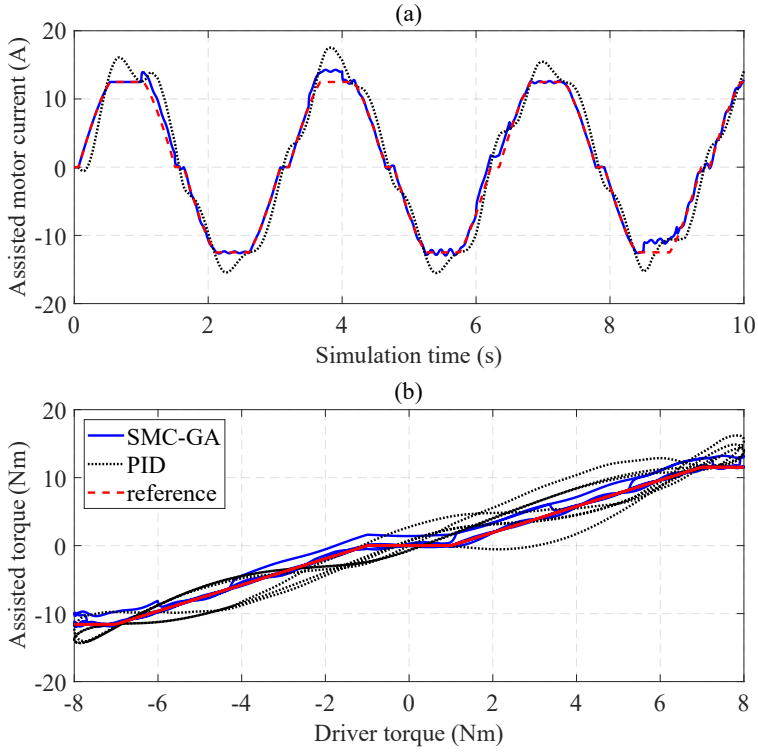

Fig. 6. Power steering performance (v_1): (a) assisted motor current, (b) assisted torque

The calculation results for the first case are summarized in Table 3. Note that these data have been rounded from the original base values.

Table 3. Simulation results (v_1)

RMS error	SMC-GA		PID failure		Failure	
	Value	Percent	Value	Percent	Value	Percent
SCA (rad)	0.004	0.109	0.319	8.278	3.034	78.717
SCS (rad/s)	0.062	0.840	0.833	11.248	5.948	80.274
SMS (rad/s)	0.409	0.301	15.072	11.080	109.813	80.731
Current (A)	0.844	9.426	2.169	24.241		

3.2. Steering at speed v_2

The following investigation is conducted when the car moves at an average speed (v_2 = 60 km/h). As the speed rises, the power assist performance declines, causing the output values to decrease. The results illustrated in Fig. 7a show that the RMS errors of the SCA are 0.203 rad and 0.005 rad for the PID and SMC-GA control, respectively. A significant decrease in the values is seen when the control system fails, increasing the RMS error to 70.355%. Under the influence of environmental disturbances, the SCS signals vibrate, leading to system errors. Looking at the window plot in Fig. 7b more closely, we can see that the RMS error increases to 9.581% for PID control and 3.382% for SMC-GA control.

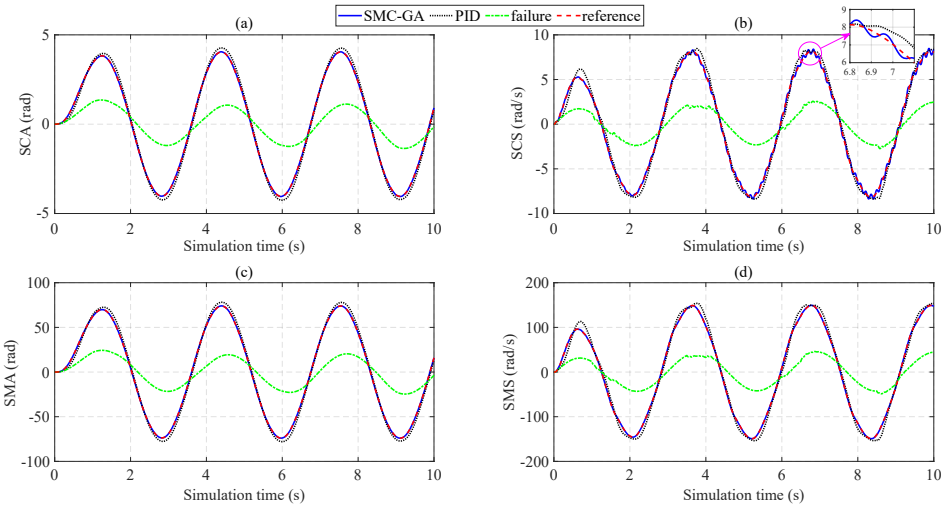

Fig. 7. Change in outputs over time (v_2): (a) SCA value, (b) SCS value, (c) SMA value, (d) SMS value

Compared to the first case, the assisted motor performance degrades as the speed increases. As a result, the assisted motor current error increases to 34.057% (PID) and 22.837% (SMC-GA) (Fig. 8a). This error is caused by the difference between the ideal and real models (the ideal model is unaffected by environmental

disturbances). Although the error of the SMC-GA controller is significantly lower than that of the PID controller, it is still considered a limitation that needs to be addressed. In this case, the assisted torque produced by the electric motor tends to track the desired signal with a small error (SMC-GA). In contrast, the error of the PID controller is more considerable, causing a severe degradation of system performance (Fig. 8b).

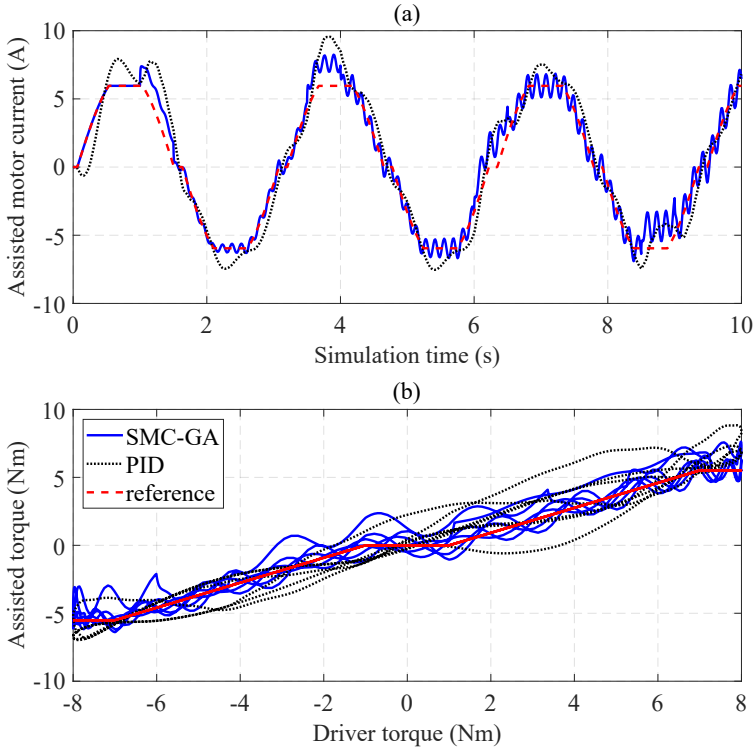

Fig. 8. Power steering performance (v_2): (a) assisted motor current, (b) assisted torque

Table 4 provides information on the results obtained in the second case. These figures have been rounded.

Table 4. Simulation results (v_2)

RMS error	SMC-GA		PID failure		Failure	
	Value	Percent	Value	Percent	Value	Percent
SCA (rad)	0.005	0.193	0.203	7.359	1.940	70.355
SCS (rad/s)	0.181	3.382	0.512	9.581	3.908	73.104
SMA (rad)	0.067	0.132	3.378	7.406	35.817	70.960
SMS (rad/s)	0.291	0.400	9.294	9.516	72.130	73.853
Current (A)	0.948	22.837	1.414	34.057		

Despite its advantages, the design process of the proposed controller presents several challenges. Selecting appropriate GA parameters such as population size and mutation probability is nontrivial, as overly large populations may increase computation time, whereas small ones can cause premature convergence. Moreover, balancing robustness and chattering suppression requires carefully defining the fitness function. Finally, real-time implementation may face hardware constraints when the computation of the GA runs concurrently with system dynamics.

4. Conclusion

This paper presents an efficient control mechanism for the EPS system. The proposed method is based on the SMC framework with sliding surface parameters optimized by the GA to improve the system's performance. Compared with some existing SMC algorithms, the structure of the proposed algorithm is more straightforward, making the calculation and practical application easier to approach. A numerical calculation is done to validate the quality of the proposed controller. The calculation results show that the system error is significantly reduced when the proposed method controls the automotive EPS system. In addition, the influence of chattering has also been largely eliminated.

Although the proposed control provides superior performance compared with conventional methods, certain drawbacks remain. The optimization process increases computational demand, which may limit real-time applicability in real applications. In addition, the control parameters are optimized for specific operating conditions. As a result, their effectiveness may decrease when vehicle dynamics vary widely. Future research will therefore focus on developing adaptive or learning-based extensions of the GA–SMC approach to enhance real-time performance and adaptability under diverse steering scenarios.

References

[1] D.N. Nguyen and T.A. Nguyen. Proposing a BSPID control strategy considering external disturbances for electric power steering (EPS) systems. *IEEE Access*, 11:143230–143249, 2023. doi: 10.1109/ACCESS.2023.3343914.

[2] L. Xia and H. Jiang. An electronically controlled hydraulic power steering system for heavy vehicles. *Advances in Mechanical Engineering*, 8(11), 2016. doi: 10.1177/1687814016679566.

[3] T.A. Nguyen. Proposing a novel nonlinear integrated control technique for an electric power steering system to improve automotive dynamic stability. *Proceedings of the Institution of Mechanical Engineers, Part K: Journal of Multi-Body Dynamics*, 238(3):445–460, 2024. doi: 10.1177/14644193241267200.

[4] D. Ramasamy. An approach for steering wheel angle evaluation without using a true power-on steering angle sensor in electric power steering systems. *Journal of the Institution of Engineers (India) Series B*, 104(3):563–568, 2023. doi: 10.1007/s40031-023-00884-1.

[5] Y. Li, Q. Feng, Y. Zhang, and Y. Nan. Dual-motor full-weight electric power steering system for commercial vehicle. *International Journal of Automotive Technology*, 20(3):477–486, 2019. doi: 10.1007/s12239-019-0045-4.

[6] V. Govender, L. Ortmann, and S. Müller. Synthesis and validation of a rack position controller for an electric power steering. *IFAC-PapersOnLine*, 50(2):253–258, 2017. doi: 10.1016/j.ifacol.2017.12.054.

[7] M.K. Hassan, N.A.M. Azubir, H.M.I. Nizam, S.F. Toha, and B.S.K.K. Ibrahim. Optimal design of Electric Power Assisted Steering System (EPAS) using GA-PID method. *Procedia Engineering*, 41:614–621, 2012. doi: 10.1016/j.proeng.2012.07.220.

[8] R.A. Hanifah, S.F. Toha, S. Ahmad, and M.K. Hassan. Swarm-intelligence tuned current reduction for power-assisted steering control in electric vehicles. *IEEE Transactions on Industrial Electronics*, 65(9):7202–7210, 2017. doi: 10.1109/TIE.2017.2784344.

[9] Z. Zheng and J. Wei. Research on electric power steering fuzzy PI control strategy based on phase compensation. *International Journal of Dynamics and Control*, 11(4):1867–1879, 2023. doi: 10.1007/s40435-022-01077-2.

[10] Y. Li, G. Wu, L. Wu, and S. Chen. Electric power steering nonlinear problem based on proportional–integral–derivative parameter self-tuning of back propagation neural network. *Proceedings of the Institution of Mechanical Engineers, Part C: Journal of Mechanical Engineering Science*, 234(23):4725–4736, 2020. doi: 10.1177/0954406220926549.

[11] Z. Fu, Y. Lu, D. Zhao, P. Yuan, and Y. Guo. A novel dual power-driven electric power steering system for electric commercial vehicles. *Advances in Mechanical Engineering*, 15(9), 2023. doi: 10.1177/16878132231200314.

[12] C. Dannöhl, S. Müller, and H. Ulbrich. H_∞-control of a rack-assisted electric power steering system. *Vehicle System Dynamics*, 50(4):527–544, 2012. doi: 10.1080/00423114.2011.603051.

[13] W.Z. Zhao, Y.J. Li, C.Y. Wang, T. Zhao, and X.Y. Gu. H_∞ control of novel active steering integrated with electric power steering function. *Journal of Central South University*, 20(8):2151–2157, 2013. doi: 10.1007/s11771-013-1719-0.

[14] M. Irmer and H. Henrichfreise. Design of a robust LQG compensator for an electric power steering. *IFAC-PapersOnLine*, 53(2):6624–6630, 2020. doi: 10.1016/j.ifacol.2020.12.082.

[15] X. Liu, H. Pang, Y. Shang, and W. Wu. Optimal design of fault-tolerant controller for an electric power steering system with sensor failures using genetic algorithm. *Shock and Vibration*, 2018:1801589, 2018. doi: 10.1155/2018/1801589.

[16] K. Yamamoto, O. Sename, D. Koenig, and P. Moulaire. Design and experimentation of an LPV extended state feedback control on Electric Power Steering systems. *Control Engineering Practice*, 90:123–132, 2019. doi: 10.1016/j.conengprac.2019.06.004.

[17] D. Lee, K.S. Kim, and S. Kim. Controller design of an electric power steering system. *IEEE Transactions on Control Systems Technology*, 26(2):748–755, 2017. doi: 10.1109/TCST.2017.2679062.

[18] T.A. Nguyen. Development of a novel integrated control strategy for automotive electric power steering systems. *IEEE Transactions on Automation Science and Engineering*, 22:926–943, 2025. doi: 10.1109/TASE.2024.3356509.

[19] T.A. Nguyen. A novel approach to the FPIBSC strategy for an electric power steering system. *Transactions of the Institute of Measurement and Control*, 47(3):555–571, 2024. doi: 10.1177/01423312241254579.

[20] X. Ma, Y. Guo, and L. Chen. Active disturbance rejection control for electric power steering system with assist motor variable mode. *Journal of the Franklin Institute*, 355(3):1139–1155, 2018. doi: 10.1016/j.jfranklin.2017.12.024.

[21] S. Na, Z. Li, F. Qiu, and C. Zhang. Torque control of electric power steering systems based on improved active disturbance rejection control. *Mathematical Problems in Engineering*, 2020:6509607, 2020. doi: 10.1155/2020/6509607.

[22] S. Kim, M. Choi, and J. Sung. Experimental verifications of electric power steering controller based on discrete-time sliding mode control with disturbance observer. *International Journal of Automotive Technology*, 24(3):883–888, 2023. doi: 10.1007/s12239-023-0072-z.

[23] D. Lee, K. Yi, S. Chang, B. Lee, and B. Jang. Robust steering-assist torque control of electric-power-assisted-steering systems for target steering wheel torque tracking. *Mechatronics*, 49:157–167, 2018. doi: 10.1016/j.mechatronics.2017.12.007.

[24] S. Lu, M. Lian, M. Liu, C. Cho, and C. Piao. Adaptive fuzzy sliding mode control for electric power steering system. *Journal of Mechanical Science and Technology*, 31(6):2643–2650, 2017. doi: 10.1007/s12206-017-0507-4.

[25] T.A. Nguyen. Designing a new integrated control solution for electric power steering systems based on a combination of nonlinear techniques. *PLoS ONE*, 19(9):e0308530, 2024. doi: 10.1371/journal.pone.0308530.

[26] M. Farbood, M. Veysi, M. Shasadeghi, A. Izadian, T. Niknam, and J. Aghaei. Robustness improvement of computationally efficient cooperative fuzzy model predictive-integral sliding mode control of nonlinear systems. *IEEE Access*, 9:147874–147887, 2021. doi: 10.1109/ACCESS.2021.3123513.

[27] M. Farbood, M. Shasadeghi, T. Niknam, and B. Safarinejadian. Fuzzy Lyapunov-based model predictive sliding-mode control of nonlinear systems: an ellipsoid recursive feasibility approach. *IEEE Transactions on Fuzzy Systems*, 30(6):1929–1938, 2022. doi: 10.1109/TFUZZ.2021.3070680.

[28] M. Baneshi, M. Farbood, A.J. Rossiter, S. Mobayen, P. Skruch, and R. Carli. Robust model predictive sliding mode control of linear parameter varying systems. *IEEE Access*, 13:64291–64304, 2025. doi: 10.1109/ACCESS.2025.3558973.

[29] T.A. Nguyen, T.T.H. Tran, and T.B. Hoang. Design a new algorithm (iL-GA) to optimize controller parameters for an automotive suspension system. *World Journal of Engineering*, 22(4):711–724, 2024. doi: 10.1108/WJE-10-2023-0444.